




## Viscous wrinkling of nonuniform sheets

Oliver McRae , Alexandros T. Oratis , and James C. Bird <sup>\*</sup>*Department of Mechanical Engineering, Boston University, Boston, Massachusetts 02215, USA*

(Received 6 August 2021; published 15 November 2021)

This paper is associated with a poster winner of a 2020 American Physical Society's Division of Fluid Dynamics (DFD) Milton van Dyke Award for work presented at the DFD Gallery of Fluid Motion. The original poster is available online at the Gallery of Fluid Motion, <https://doi.org/10.1103/APS.DFD.2020.GFM.P0027>.

DOI: [10.1103/PhysRevFluids.6.110506](https://doi.org/10.1103/PhysRevFluids.6.110506)

Wrinkling of viscous sheets is a phenomenon with implications in both natural and applied settings, ranging from volcanology to glass manufacturing. When compressed at sufficiently fast time scales, viscous sheets can exhibit mechanical instabilities, such as wrinkling, which are typically found in elastic sheets. An aesthetically beautiful example of viscous wrinkling can be observed when a large air bubble resting on the surface of a very viscous liquid is punctured at its apex [1,2]. As the bubble collapses due to surface tension [3], it adopts a wrinkled pattern around its periphery, which is reminiscent of the wrinkling instability of elastic sheets [4,5]. Because the energetic cost of compression is much larger compared to bending, thin elastic and viscous sheets are prone to wrinkle, with the sheet thickness playing a crucial role in setting the wrinkled pattern. However, the thickness of the viscous film during the bubble collapse is nonuniform, an element absent from most wrinkling studies on elastic sheets. Here, we visualize the bubble collapse with high-resolution images and demonstrate how analyzing the interference patterns provides insight into how the film thickness varies as the wrinkles develop.

The collapse and wrinkling instability of a viscous bubble is illustrated in Fig. 1(a). Air is injected with a hypodermic needle below the surface of a 2500 Pa s silicone oil bath. The air bubble rises to the surface and forms a hemispherical dome with radius  $R_0 \approx 1.5$  cm. As the bubble rests on the liquid surface, it is manually punctured at its apex with a 25-gauge needle [6]. The puncture results in the expansion of a hole that grows exponentially within milliseconds until it meets a thicker region along the bubble's interface [1]. Simultaneously, the bubble collapses downward toward its base during which wrinkles develop around its edge from sufficiently fast compression rates in the radial direction [3]. Within a second, the initially spherical bubble deforms into a disk with three distinct regions: the punctured hole, followed by a smooth sheet, and the wrinkled region [Fig. 1(a), 1.00 s]. The bubble collapse was captured at eight frames per second with a 200-mm prime lens on a Nikon D7500 at 20.9 megapixels with ISO 200, f-stop 25, and shutter speed 1/125 s. The light sources and their positioning are described in greater detail in a previous Science Visuals article [6]. A closer examination of the unwrinkled sheet highlights the presence of concentric interference fringes [Fig. 1(b)], a hallmark of a nonuniform thickness along the radial direction  $r$ .

---

\*jbird@bu.edu

Published by the American Physical Society under the terms of the [Creative Commons Attribution 4.0 International](https://creativecommons.org/licenses/by/4.0/) license. Further distribution of this work must maintain attribution to the author(s) and the published article's title, journal citation, and DOI.

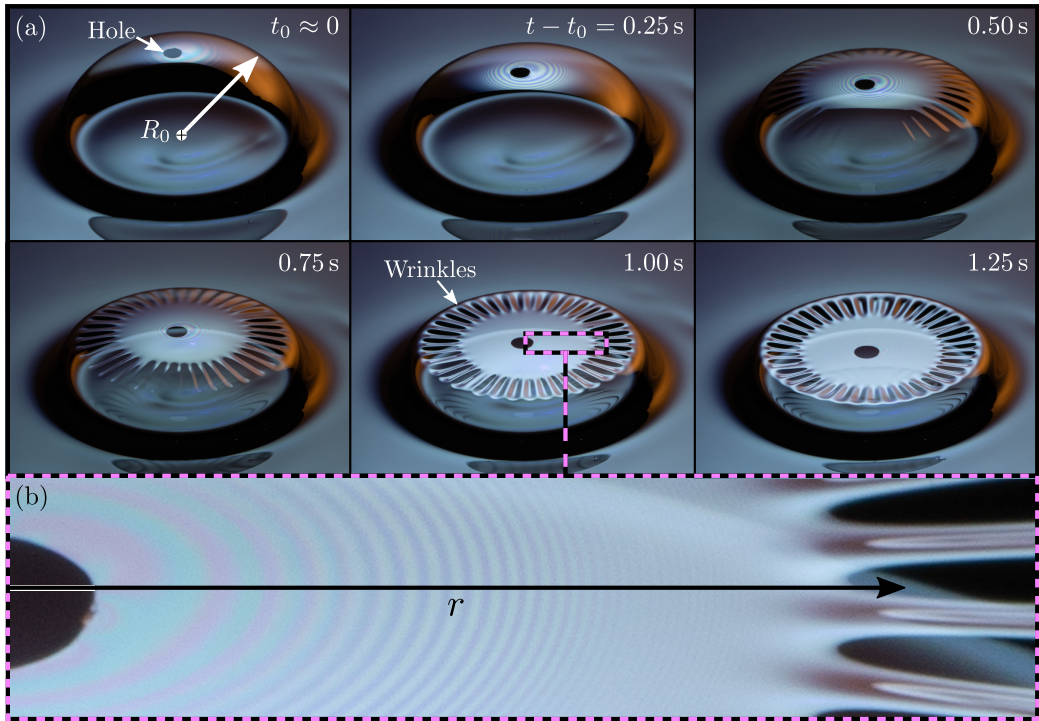


FIG. 1. Collapse and wrinkling of a viscous bubble. (a) When a bubble with radius  $R_0$  is punctured on the surface of a 2500 Pa s silicone oil bath, it collapses toward its base within seconds. During the collapse, a wrinkled pattern emerges around the bubble's periphery. The wrinkles around the bubble's edge are separated from the punctured hole by a smooth viscous sheet. (b) A closer inspection of the smooth region reveals the presence of concentric interference fringes along the radial direction  $r$ , which highlights a nonuniformity in the sheet's thickness.

To quantify the nonuniformity of the film thickness, we measure the intensity of the interference fringes. RAW files from the camera are converted after white balancing to RGB images. Each pixel in an RGB image is composed of three channels: red, green, and blue. The brightness of each channel ranges from 0 to 255, with (0,0,0) and (255,255,255) corresponding to black and white, respectively. The pixel-by-pixel red, green, and blue channel intensity values are extracted along a horizontal line that spans from the center of the concentric fringes to  $0.6R_0$ . Figure 2 plots the brightness intensity values as a function of radial position  $r$  normalized by the initial bubble radius  $R_0$  for the six images shown in Fig. 1(a). The brightness intensity curves at times 0.50 and 1.00 s are plotted over the corresponding spatially matched images [Fig. 1(a)] from which the intensity values were extracted. For clarity, the intensities for all three color channels are only included for the plot corresponding to the second image. As expected, the wavelength for these fringes varies with color frequency, and the relative position of the peaks may offer insight into the absolute thickness. Due to lighting, the red channel offers the most stable output across all six images and is presented here for comparative purposes. To sharpen the fringes, the intensity data for the later times is smoothed using a moving average with a span of five data points. With the aid of visual guidelines (dashed lines in Fig. 2), we observe that over time, the radial position of the hole and first fringe moves outward, the third fringe remains roughly stationary, and the tenth fringe moves inward. Although we do not report an absolute thickness nor account for curvature in our radial positions, the degree to which the fringes converge over time suggests that the bubble film compresses in this unwrinkled region, and consequently becomes thicker. Furthermore, the

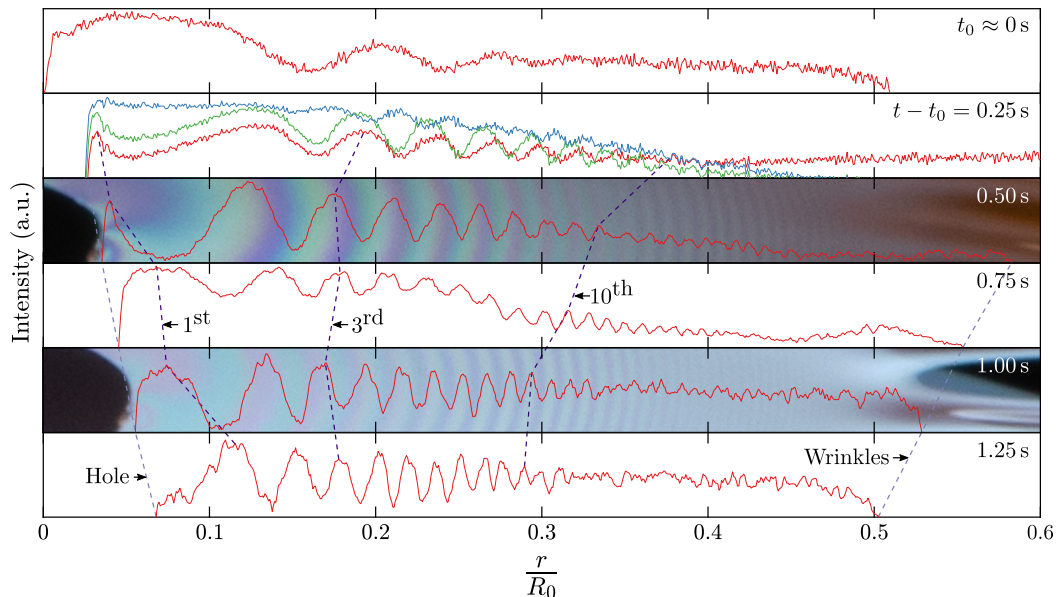


FIG. 2. Spatiotemporal evolution of bubble film interference fringes as recorded from red-green-blue components of pixels of the region outlined in Fig. 1(b). Brightness intensity values at the six distinct times in Fig. 1(a) for the pixels along a horizontal radial line from the center of the collapsing top of the bubble are plotted. All three color channels are plotted at time 0.25 s; however, for clarity, only the red channel is plotted at the other times. Note that the radius of the hole increases throughout the collapse but remains less than 5% the radius of the bubble. The curves reveal interference fringes as regular peaks and valleys, the positions of which can be compared at different instances in time. The outward movement of the first fringe and the inward movement of the tenth fringe suggest an overall compression and thickening of the unwrinkled region of the bubble film.

number of fringes between the hole and the wrinkles is approximately 30 [Fig. 1(b)]. Assuming that each fringe corresponds to a thickness variation of approximately half the wavelength of light, or 350 nm, the difference in thickness between the hole and wrinkles would be approximately 10.5  $\mu\text{m}$ .

Despite the similarities between the wrinkles in viscous and elastic sheets, a key difference in the location of the wrinkles was attributed to the thickness variation in the viscous sheet [3]. Specifically, the smooth region between the hole and wrinkles was attributed to the film being sufficiently thin for surface tension to suppress viscous buckling. Our results provide evidence that the film thickness is at least 10  $\mu\text{m}$  where wrinkles develop, even when the hole dynamics are consistent with a bubble apex thickness of around 1  $\mu\text{m}$ . Moreover, our results demonstrate that the radial thickness variation increases as the bubbles collapse. Our elementary approach is a first step toward more precise measurements of the thickness variation of a collapsing viscous film with the ultimate goal of uncovering how the thickness nonuniformity affects the wrinkling pattern. Given that similar interface patterns are observed on silicone oils over a range of viscosities [3], we anticipate that our findings generalize beyond this particular liquid. In addition to documenting quantitative trends, the data provided here may help validate analytic and numeric models of the curved viscous film collapse.

We thank Bill Douthitt for helpful conversations around the imaging process. This work was partially supported by National Science Foundation Grant No. 1351466 and Office of Naval Research Grant No. N00014-16-1-3000. Any opinions, findings, and conclusions or recommendations

expressed in this material are those of the authors and do not necessarily reflect the views of the funding agencies.

---

- [1] G. Debrégeas, P.-G. de Gennes, and F. Brochard-Wyart, The life and death of “bare” viscous bubbles, *Science* **279**, 1704 (1998).
- [2] R. da Silveira, S. Chaïeb, and L. Mahadevan, Rippling instability of a collapsing bubble, *Science* **287**, 1468 (2000).
- [3] A. T. Oratis, J. W. Bush, H. A. Stone, and J. C. Bird, A new wrinkle on liquid sheets: Turning the mechanism of viscous bubble collapse upside down, *Science* **369**, 685 (2020).
- [4] B. Davidovitch, R. D. Schroll, D. Vella, M. Adda-Bedia, and E. A. Cerda, Prototypical model for tensional wrinkling in thin sheets, *Proc. Natl. Acad. Sci. U.S.A.* **108**, 18227 (2011).
- [5] H. King, R. D. Schroll, B. Davidovitch, and N. Menon, Elastic sheet on a liquid drop reveals wrinkling and crumpling as distinct symmetry-breaking instabilities, *Proc. Natl. Acad. Sci. U.S.A.* **109**, 9716 (2012).
- [6] B. Douthitt, Ripple Effects, 2020, <https://www.science.org/content/blog-post/ripple-effects>.